CCD PHOTOMETRY AND TIME SERIES ANALYSIS OF V2275 CYG AND RW UMI USING DATA FROM THE TUBITAK NATIONAL OBSERVATORY

A THESIS SUBMITTED TO
THE GRADUATE SCHOOL OF NATURAL AND APPLIED SCIENCES
OF
MIDDLE EAST TECHNICAL UNIVERSITY

BY

MUSTAFA ARDA YILMAZ

IN PARTIAL FULFILLMENT OF THE REQUIREMENTS

FOR

THE DEGREE OF MASTER OF SCIENCE

IN

PHYSICS

AUGUST 2004

Approval of the Graduate School of Natural and Applied Sciences.

Prof. Dr. Canan Özgen
Director

I certify that this thesis satisfies all the requirements as a thesis for the degree of Master of Science.

Prof. Dr. Sinan Bilikmen
Head of Department

This is to certify that we have read this thesis and that in our opinion it is fully adequate, in scope and quality, as a thesis for the degree of Master of Science.

Assoc. Prof. Dr. Şölen Balman
Supervisor

Examining Committee Members

Prof. Dr. Nilgün Kızıloğlu (METU, PHYS) _____

Assoc. Prof. Dr. Şölen Balman (METU, PHYS) _____

Assist. Prof. Dr. Fatma Gök (Akdz.U, PHYS) _____

Prof. Dr. Halil Kırbıyık (METU, PHYS) _____

Prof. Dr. Ümit Kızıloğlu (METU, PHYS) _____

I hereby declare that all information in this document has been obtained and presented in accordance with academic rules and ethical conduct. I also declare that, as required by these rules and conduct, I have fully cited and referenced all material and results that are not original to this work.

Mustafa Arda Yılmaz

ABSTRACT

CCD PHOTOMETRY AND TIME SERIES ANALYSIS OF V2275 Cyg AND RW UMi USING DATA FROM THE TUBITAK NATIONAL OBSERVATORY

YILMAZ, Mustafa Arda

M.S., Department of Physics

Supervisor: Assoc. Prof. Dr. Şölen Balman

August 2004, 39 pages.

In this work, we analyze the data from 1.5 m telescope of Tubitak National Observatory (TUG) for two objects V2275 Cyg and RW UMi. After applying aperture and PSF photometry to the CCD data, we derive the light curve of the objects. Also we apply discrete Fourier transform and Scargle time series analysis to obtain power spectrum and search for periodicities in their power spectra in which both systems show interesting properties. We discover large variations in V2275 Cyg due to irradiation effects on the secondary, with an orbital period $P_{orb} = 0.316 \pm 0.007$ day. We also detect a very short orbital period for RW UMi $P_{orb} = 1.96 \pm 0.073h$ and also a spin period $P_{spin} = 1.29 \pm 0.036h$ in the presence of several beat frequencies. These results (if confirmed) lead us to say that RW UMi can be an intermediate of polar system.

Keywords: CCD Photometry, cataclysmic variables, classical novae, time series analysis, V2275 Cyg, RW UMi.

ÖZ

TUBİTAK ULUSAL GÖZLEMEVİ VERİLERİNİ KULLANARAK V2275 Cyg VE RW UMi'nin CCD FOTOMETRİSİ VE ZAMAN SERİSİ ANALİZİ

YILMAZ, Mustafa Arda
Yüksek Lisans , Fizik Bölümü
Tez Yöneticisi: Doç. Dr. Şölen Balman

August 2004, 39 sayfa.

Bu tezde, V2275 Cyg ve RW UMi adlı kataklizmik değişkenler için 1.5 m'lik TUBİTAK ULUSAL GÖZLEMEVİ (TUG) teleskobu kullanılarak alınan verilerin çözümlemesi yapılmıştır. CCD verilerine açıklık ve PSF fotometrisi uygulandıktan sonra kaynakların ışık eğrileri çıkarılmıştır. Bu iki sistemin zaman serilerinin güç tayfı Scargle ve ayrık Fourier dönüşümleri kullanılarak yapılmıştır. V2275 Cyg kaynağında ikincil yıldızın üzerindeki beyaz cüceden gelen ışımanın yol açtığı ısınma etkisinden kaynaklanabilecek olan büyük kadir değişimleri $P = 0.316 \pm 0.007$ gün'lük yörünge dönemi ile birlikte tespit edilmiştir. İkinci olarak RW UMi için çok kısa bir yörünge dönemi $P = 1.96 \pm 0.073$ s, ek olarak vuru frekansı ve yan bant frekansları ile birlikte beyaz cüce dönme dönemi $P = 1.29 \pm 0.036$ s bulunmuştur. Bu sonuçlar doğrulandığı taktirde RW UMi'nin orta dereceli manyetik alanlı kataklizmik değişken tipi bir sistem olduğu söylenebilir.

Anahtar Sözcükler: CCD Fotometri, kataklizmik değişkenler, klasik novalar, zaman serisi analizi, V2275 Cyg, RW UMi

To My Family...

ACKNOWLEDGMENTS

I am deeply indebted to my supervisor Assoc. Prof. Dr. Şölen Balman for her guidance, encouragement, invaluable comments, patience, continuous support and friendly attitude during this work. Thank you sincerely.

There are no words to describe the appreciation and gratitude I fell for my parents. Their wonderful example of dedication and commitment has provided me with a lifetime of inspiration. I thank them for their optimism, beautiful spirits and belief in me. I also wish to express my appreciation to my brother and his wife. They patiently and lovingly encouraged me to do my best.

I am grateful to my friends Vedat, Tamer and Rengin for their invaluable support and friendship. Also special thanks to all astro group. I could not have completed this thesis without you.

Thank you all very much indeed.

TABLE OF CONTENTS

PLAGIARISM iii

ABSTRACT iv

ÖZ v

DEDICATON vi

ACKNOWLEDGMENTS vi

TABLE OF CONTENTS viii

LIST OF TABLES x

LIST OF FIGURES xi

CHAPTER

1 INTRODUCTON 1

2 CHARGED COUPLE DEVICES (CCD) AND BASIC PHOTOMETRY TECHNIQUES 9

2.1 Brief Information About CCD 9

2.2 Common Noise Sources 10

2.3 Basic Reductions 12

2.4 Basic Photometry Techniques 13

2.4.1 Aperture Photometry(AP) 13

2.4.2 Image Center Determination 13

2.4.3 Background Determination 15

2.4.4 Adding Up The Light 16

2.4.5 Point Spread Function Photometry (PSF) 16

2.4.6 Transformation To A Standard System 16

3 TIME SERIES ANALYSIS AND POWER SPECTRAL METHODS 18
3.1 Discrete Fourier Transform 18
3.2 Scargle Time Series Analysis 23

4 PHOTOMETRIC ANALYSIS OF V2275 CYG AND RW UMI . . 24
4.1 Photometric Analysis of V2275 Cyg 24
4.2 Photometric Analysis of Classical Nova RW UMi 29

5 CONCLUSION 36

REFERENCES 38

LIST OF TABLES

4.1 The observations time table for V2275 Cyg 26
4.2 The observations time table for RW UMi 30
4.3 Detected significant frequencies and corresponding periods for RW UMi 32

LIST OF FIGURES

1.1 A diagram of a Cataclysmic Variable, showing the normal star, the accretion disk, and the white dwarf. The hot spot is where matter from the normal star meets the accretion disk. 2

1.2 The Roche equipotentials. 3

1.3 A typical morphology of a nova light curve (from Warner 1989). . 5

1.4 Light curves of several novae in outburst (from Warner 1989). Intervals are of one magnitude and ten days. 6

1.5 The CNO nuclei and interactions of the CNO cycle. The abscissa is the atomic mass and the ordinate is the atomic number (e.g. the number of protons in the nuclei). Above 10^8 K, the decay of the β^+ unstable nuclei becomes the limiting factor in the cycle. 8

1.6 Nova Cygni 1992. 8

3.1 99% (dashed lines) 90% (solid lines) confidence levels for different MW's. 22

4.1 The field of the classical nova (V2275 Cyg). The nova is circled. The image was obtained on 2002.12.22. North is up, east is left. . 24

4.2 The light curve of V2275 Cyg obtained using the 1.5m telescope at TUG with R filter during the 4 nights in 2002 October. Errors are also included. 25

4.3 The light curve of V2275 Cyg obtained using the 1.5m telescope at TUG with R filter during the 8 nights in 2002. Errors are also included. 26

4.4 Power spectrum of V2275 Cyg obtained performing a transform of the entire time series data using the Scargle algorithm. 27

4.5 The field of the classical nova (RW UMi). The nova is circled. The image was obtained on 2001.09.16. North is up and east is left. . . 29

4.6 The light curve of RW UMi obtained using the 1.5m telescope at TUG and 1m telescope at WISE observatory with R filter during the 14 nights. Errors are also included. 31

4.7 Power spectrum of RW UMi obtained performing a transform of the time series data obtained by R filter using the Scargle algorithm. 33

4.8 Power spectrum of RW UMi obtained performing a transform of the time series data obtained by clear filter using the Scargle algorithm. 33

4.9 Power spectrum of RW UMi obtained performing a transform of the time series data obtained by combination of R and clear filter using the Scargle algorithm. 34

4.10 Power spectrum of RW UMi obtained performing a transform of the time series data obtained by V filter using the Scargle algorithm. 34

4.11 Power spectrum of RW UMi obtained performing a transform of the entire time series data using the Scargle algorithm. 35

CHAPTER 1

INTRODUCTON

Cataclysmic variables (CVs) (Fig.1.1) are short period close interacting binary stars. They are composed of a low mass main sequence star -i.e.,called secondary- which fills its Roche lobe (Fig.1.2) and a white dwarf (primary), which accreted material from its companion through an accretion disc that surround itself. The Roche lobe is a region where the gravitational potential of the system is common between the two stars . As the secondary star expands, which happens in normal stellar evolution, it fills it's Roche lobe and from that point it will accrete on to the primary. With this infall of gas towards the primary, it forms an accretion disc because it has angular momentum and so cannot fall directly onto the star. With this angular momentum it whips past the secondary and forms a circle of gas around the star - inside the roche lobe. With this process happening all the time, more and more gas gets 'ejected' into the ring and viscosity causes the gas to lose angular momentum (there is a frictional torque on the disc), which also heats it up, allowing the matter in the disc to spiral down onto the primary. For two large co-orbiting bodies with nearly circular orbits of masses m_1 and m_2

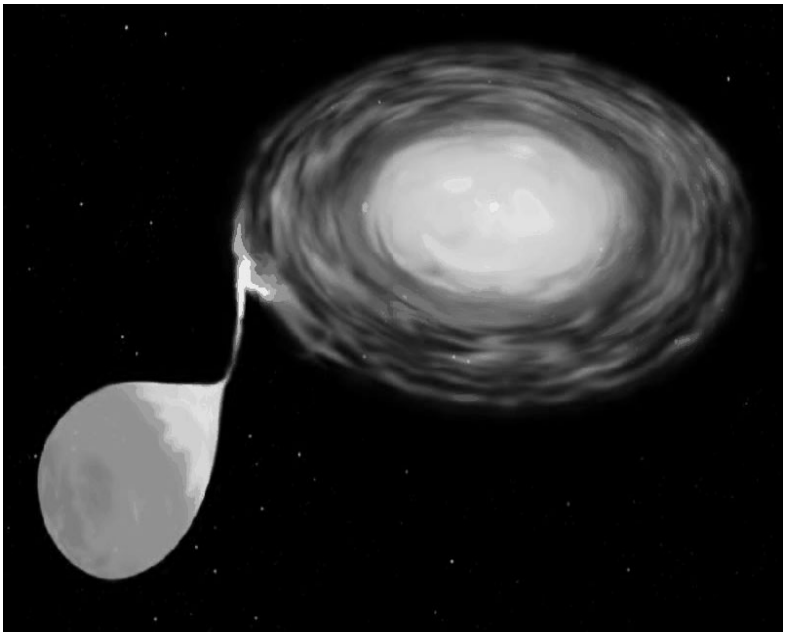

Figure 1.1: A diagram of a Cataclysmic Variable, showing the normal star, the accretion disk, and the white dwarf. The hot spot is where matter from the normal star meets the accretion disk.

(with $m_1 < m_2$), and a third small body having the same revolution period n as the other two, there are five points where the gravitational forces of the two large bodies exactly balance the centrifugal force felt by the small body. The points are called Lagrange points, and an object placed at one of these points would remain in the same position with respect to the other two. These five Lagrange points are also called equilibrium points. L_4 and L_5 are stable points which are at the vertices of an equilateral triangle whose base is the m_1m_2 line, where L_1, L_2 and L_3 are unstable points.

CVs are classified mainly into two groups: non-magnetic CVs and magnetic CVs. Non-magnetic CVs are categorized by their outburst characteristics as,

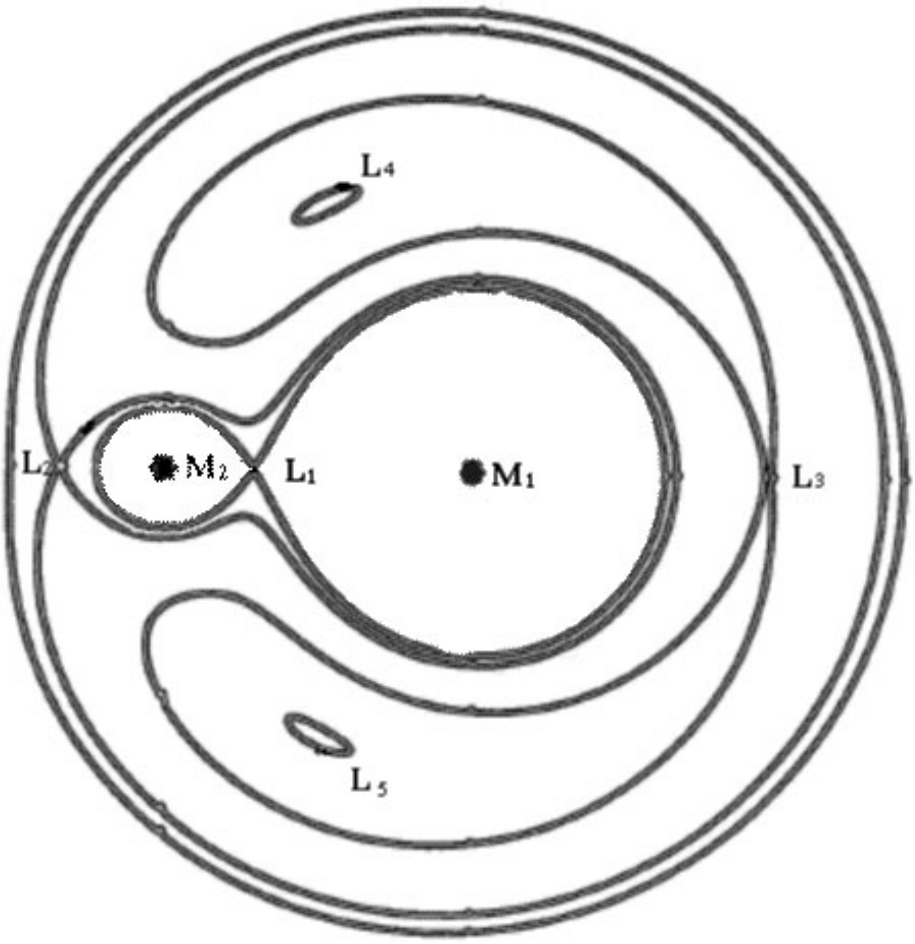

Figure 1.2: The Roche equipotentials.

Classical Novae, Dwarf Novae, Recurrent Novae and Nova-like variables. Dwarf novae (DN) have outbursts with 2 to 5 mag which lasts between 10 days to tens of years. They have three subclasses: Z Cam, SU UMa, U Gem. Recurrent novae look like classical novae but they repeat their eruptions and they are distinguished from DN by the ejected shell during their outburst. DN are not known to have mass loss in their outburst stage. Magnetic CVs have two subclasses according to their magnetic field strength: (1) *polars* which have strongest magnetic fields

and (2) *intermediate polars* which have weaker fields. Our focus is classical novae in this work.

If the system is non-magnetic, i.e., the magnetic field of WD is weak, the matter transferring from secondary to primary through accretion disc spirals down to the surface of the WD. But, if the system is magnetic the disk becomes truncated and matter falls onto the WD following magnetic field lines at the Alfven radius. Gas which is falling towards a magnetized star is resisted by the magnetic field. The volume within which magnetic field affects the flow of mass ,energy and angular momentum is called magnetosphere (Lamb, 1986). The radius where the gas pressure in the accreting gas is equal to the magnetic pressure of magnetosphere of the WD is called the Alfven radius. We can calculate the Alfven radius as

$$\tau_A = 9.9 \times 10^{10} \mu_{34}^{4/7} M_1^{-1/7} \dot{M}_{16}^{-2/7} cm \tag{1.1}$$

where M_1 is the mass of the WD in solar mass units, $\dot{M}_{16}$ is the accretion rate in $10^{16} gr/s$, μ_{34} is the magnetic moment of the WD in units of $10^{34} Gcm^3$

Classical novae are characterized by their sudden increase in brightness, of the order 6 to greater than 19 magnitudes (Warner,B. 1995) and have only one observed eruption. We can define classical novae as fast or slow by their decline rate after their rapid rise in luminosity(Payne-Gaposchkin 1957). For the first few months the bolometric luminosity stays nearly constant while the visual luminosity decreases. We can see the typical morphology of a nova light curve in

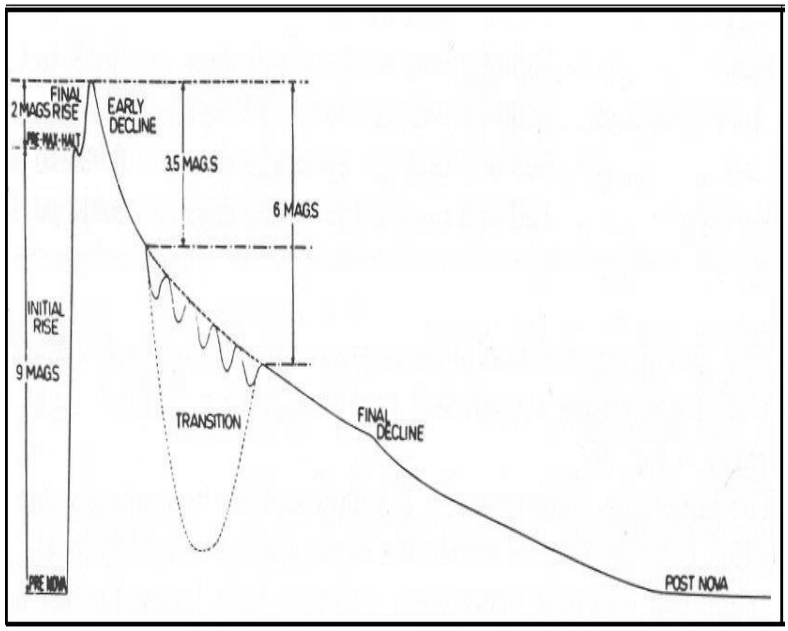

Figure 1.3: A typical morphology of a nova light curve (from Warner 1989).

Fig.1.3 and light curves of several novae in outburst in Fig.1.4 (Warner 1989).

The hot gas accreting on the surface of a white dwarf is heated and compressed. The hydrogen rich disc material and the material of the white dwarf which is composed of carbon, oxygen and nitrogen are mixed by turbulent motions in the region between the surface and the accreting matter. This region is called core accretion envelope boundary(CAEB). As more and more material accreted on the WD, the temperature and pressure increases at the envelope. When the temperature reaches about 10^7K, proton-proton chain begins. In p-p chain, when the energy increases, the temperature also increases which again leads to an increase in energy. In an ordinary star thermal pressure is dominant and this energy production is regulated by expansion of the star in radius. However,

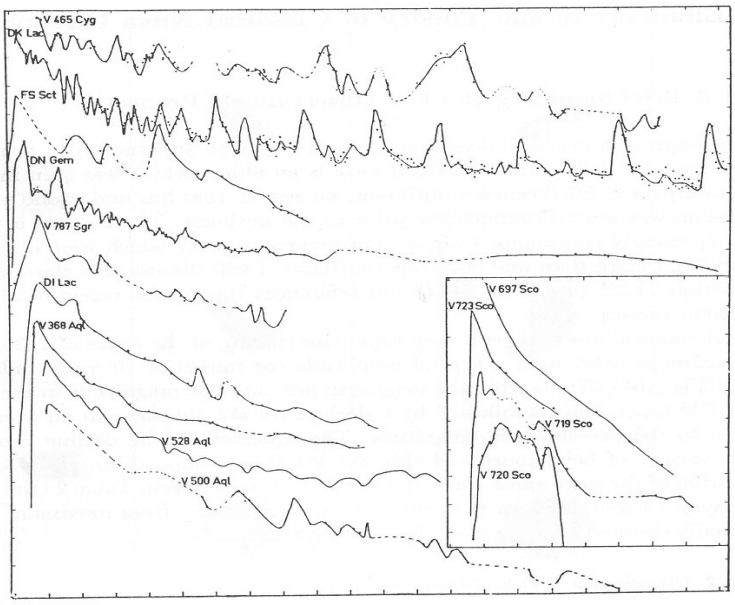

Figure 1.4: Light curves of several novae in outburst (from Warner 1989). Intervals are of one magnitude and ten days.

WDs are degenerate stars in which the electron degeneracy pressure is dominant. Since most of the electrons are in Fermi levels under very high pressure and temperature, its very difficult to make them free. So when the temperature increases, the degenerate gas does not expand. Resulting a continuous increase in the energy production. This process is called thermonuclear runaway (TNR). The energy in nova outburst is generated by the hot CNO cycle (Fig. 1.5 (Starrfield et al. 1972). Theoretical calculations show that the β^+ unstable nuclei (N^{13}, O^{14}, O^{15}, F^{17}) are very important in the outburst. In the hot burning shell($\sim 10^8$) the life time of proton captures becomes shorter than the decay times. The decay times of β^+ unstable nuclei are 863 s, 102 s, 176 s and 92 s respectively. This makes the β^+ unstable nuclei most abundant CNO nuclei in the shell. Additionally,

envelope become convective as the temperature increases. This causes β^+ nuclei is transported to the upper part of the surface layers. Because the convective turnover time scale is about 10^2 s which is shorter than the decay times. Then β^+ nuclei decay produce a large amount of energy in the surface (10^{46} ergs) which is comparable with the binding energy of the envelope. This results a shock which ejects the material out into the space. This is called nova outburst. Figure 1.6 belongs to object Nova Cyg 1992, photographed by Hubble Space Telescope showing the material ejected by the WD of the system.

Some CVs show an interesting photometric property in during dwarf nova and classical outbursts which is called superhump. Superhump periods are a few percent (1-10) larger or smaller than the orbital period of the binary system so they are called positive(apsidal) or negative(nodal) respectively. There are systems where we can observe both the positive and negative superhumps so we can conclude that they have different mechanisms. The former is tidal resonance between material orbits in the disk and secondary star, with 3:1 commensurability (Whitehurst and King 1990), while latter is due to the retrograde precession of a distorted accretion disk tilted above the orbital plane(Harvey et al 1995). Superhumps have an important role in order to determine the mass accretion history of the systems and the mass of the white dwarfs.

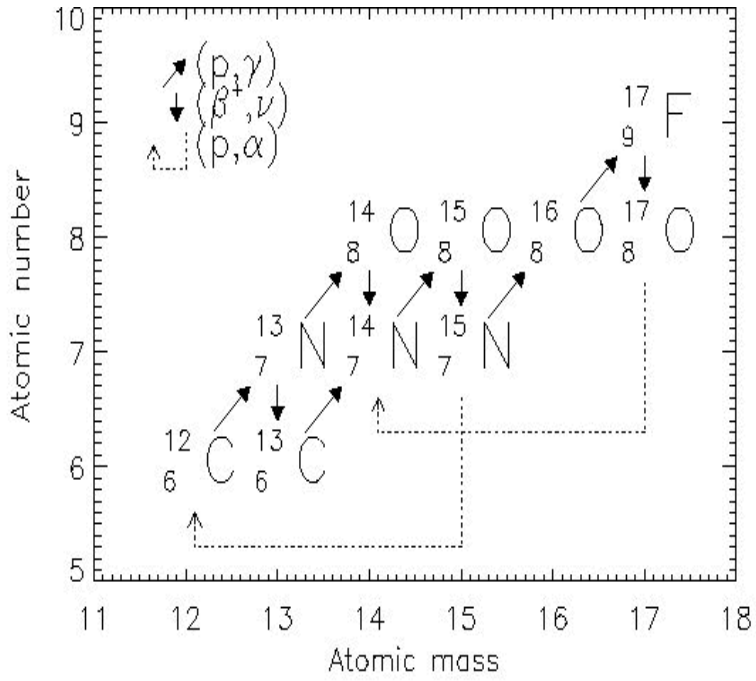

Figure 1.5: The CNO nuclei and interactions of the CNO cycle. The abscissa is the atomic mass and the ordinate is the atomic number (e.g. the number of protons in the nuclei). Above 10^8 K, the decay of the β^+ unstable nuclei becomes the limiting factor in the cycle.

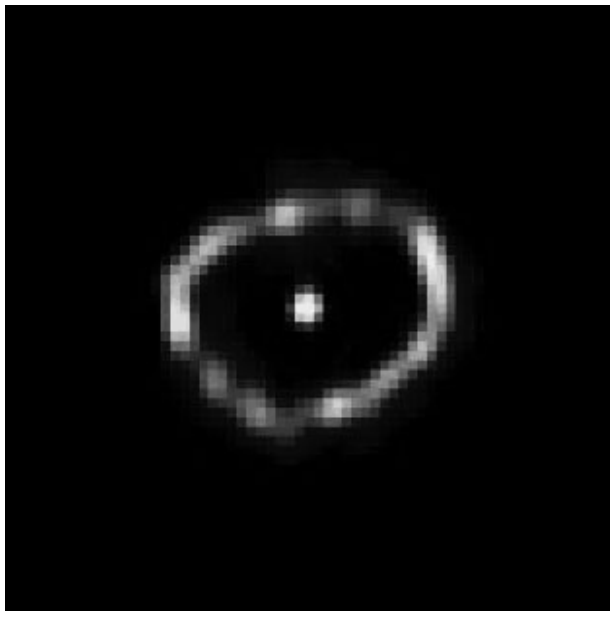

Figure 1.6: Nova Cygni 1992.

CHAPTER 2

CHARGED COUPLE DEVICES (CCD) AND BASIC PHOTOMETRY TECHNIQUES

2.1 Brief Information About CCD

Charge-coupled devices (CCDs) were first introduced to the world in 1970 in a pair of papers by Boyle and Smith in the Bell System Technical Journal. Basically they are photon counting devices that estimate the number of photons counted. There are four steps in order to generate a CCD image (Howell 1992).

1.Charge Generation: This step consists of the photoelectric effect. Incoming photons can interact with the silicon atoms and excite valance electrons into the conduction band creating electron-hole (e-h) pairs. The e-h pairs created are free to move and diffuse in the silicon lattice structure.

2.Charge Collection: In this step the photoelectrons are collected in the collecting sites or pixels. The collection sites are defined by electrodes formed on the CCD. These electrodes are called gates.

3.Charge Transfer: Manipulating the voltage systematically, signal electrons move down the vertical registers from one pixel to the following. Then

a horizontal register of pixels collects the signal electrons a line at a time and transports the charged packets to an amplifier.

4.Charge Detector: In the last step, charge packets are converted to an output voltage. Then, these voltages are amplified and digitally encoded. By using a computer these are displayed on a monitor. CCD data values are initially in digital numbers (DN), equal to the number of electrons (photons detected) divided by the number of electrons per ADU. The number of counts read out is ADU.

2.2 Common Noise Sources

There are several noise sources that is encountered in the CCD data. In order to calibrate the CCD data we must reduce noises in the data. Here are some of the noise sources:

a) Poisson Fluctuations: These are natural and basic noise source. It can be calculated from the probability distributions.

b) Gain Variations (flat-field): Every pixel have different quantum efficiencies depending on the structural variations on the CCD. It is the ratio of striking electrons and recorded electrons. If we expose the CCD to a uniform illumination, and take a well exposed integration, resulting pixel to pixel variations directly reflect the quantum efficiency differences.

c) Cosmic Ray Induced Electrons: Cosmic rays striking the CCD continuously, create hot pixels. This is detected as very bright dots on the image.

d) Read Noise: The charge level for each CCD pixel is measured in turn by an output amplifier, however the system misses some of the photoelectrons in each pixel. The number of photoelectrons which remain in the pixel is defined as read noise.

e) Dark Current: When the CCD exceeds the operational temperature, new photoelectrons appear. Measurement of dark current is usually done by taking several long exposures when the shutter of the CCD camera is closed.

f) Bias Level: Because the system has its own electric, although there isn't any income to the CCD, it creates an electron flat by itself. For most of the CCD detector systems this is not an important noise source.

g) Saturation : When the source is too bright, depending on the integration time, it creates an overflow in the pixels. For this reason, the star profiles become flat topped and the data cannot be used.

In order to determine the true photon rate of a light source, we must calculate the signal-to-noise rate in a proper integration time.

$$S/N = N_c/\sqrt{N_c + n_{pix}(N_s + N_d + N_r^2)} \tag{2.1}$$

N_c : total electron number

N_s : sky number

N_d : dark noise number

N_r : read noise number

2.3 Basic Reductions

Before performing the photometric analysis of CCD data, we must clean the noise sources from the data. First, we assume the data as a 2x2 matrix (I_{ij}). Then, we subtract the dark current (D_{ij}) from the data.

$$I'_{ij} = I_{ij} - (B_{ij}) - D_{ij} \tag{2.2}$$

Bias (B_{ij}) correction is optional and this is often not required. The D_{ij} must be scaled to the correct relative exposure time of the data frame.

$$G'_{ij} = G_{ij} - D_{ij} \tag{2.3}$$

The dark corrected gain should be normalized to its mean counts before division with the data frame in order to correct for pixel to pixel variations.

$$G''_{ij} = G'_{ij} / < G'_{ij} > \tag{2.4}$$

In general during the derivation of individual calibration frames all previous reduction steps should be applied. For example, if the I_{ij} is to be D_{ij} subtracted then the gain variations G_{ij} should be dark subtracted also.

$$I''_{ij} = I'_{ij} / G''ij \tag{2.5}$$

We normalize the dark corrected data by dividing it to dark corrected gain and obtain reduced I''.

2.4 Basic Photometry Techniques

2.4.1 Aperture Photometry(AP)

This technique works very well if the field of interest is not too crowded. In order to use this technique, we must determine the image center and sky background. First, pixels that contain light from the star are added up. After that, we determine the sky background contribution to the pixels using near by pixels and subtract this to find the net signal. Since the summation of light from the star is usually done within a circular aperture, this technique is known as *aperture photometry*. There are three steps to derive the magnitude: stellar image center determination, estimating the sky background and calculating total amount of light from the star.

2.4.2 Image Center Determination

There are two methods; one of them is marginal sum method, the other is image centroiding method.

i) Marginal Sum Method: In this method, we first guess an initial center for the star. Then we form a subarray. The size of the subarray should be large i.e. at least 5 times of the full width at half maximum of the star image in size.

Then, we sum up the pixel intensities as below;

$$\rho(x_i) \quad = \quad \sum_j I_{ij}$$

$$\rho(y_j) \;=\; \sum_i I_{ij} \tag{2.6}$$

$\rho(x_i)$ and $\rho(y_i)$ are marginal sums. I_{ij} is the intensity at the pixel. After that we fit a Gaussian function to these marginal sums so that we find an image center in each coordinate. If the star of interest is isolated, this technique works perfectly, however if the star has near by companions that fall within the subarray, then the technique goes wrong.

ii) Image Centroiding Method: First part of this method is the same as the marginal sum method, however this time we don't use the whole subarray, instead of this the sum is confined to a 2a x 2a box. Here a refers to the full width at half maximum.

Then, the marginal sums become;

$$\begin{aligned} \rho(x_i) &= \sum_{j=-a}^{a} I_{ij} \\ \rho(y_j) &= \sum_{i=-a}^{a} I_{ij} \end{aligned} \tag{2.7}$$

Afterwards, we compute the mean intensities;

$$\begin{aligned} < x > &= \frac{1}{2a+1} \sum_{i=-a}^{a} \rho(x_i) \\ < y > &= \frac{1}{2a+1} \sum_{j=-a}^{a} \rho(x_j) \end{aligned} \tag{2.8}$$

Using these mean intensities the new center of star is computed like this;

$$\begin{aligned} x_1 &= \frac{\sum_{i=-a}^{a}(\rho(x_i) - < x >)x_i}{\sum_{i=-a}^{a}(\rho(x_i) - < x >)} \\ y_1 &= \frac{\sum_{j=-a}^{a}(\rho(y_j) - < y >)y_j}{\sum_{j=-a}^{a}(\rho(y_j) - < y >)} \end{aligned} \tag{2.9}$$

If the new center is as close as one pixel to the initially estimated center, the center is correct, else the new center becomes the initial center and the procedure is iterated until the correct center is found.

2.4.3 Background Determination

To determine the background, we look at the signal in an annular region centered on the star. In order to make the uncertainty in the background smaller we should take the inner radius of the annulus sufficiently larger (several times the FWHM) so that it contains many pixels. The pixels in the sky annulus show Gaussian distribution. In ideal situations we can take the mean value of the Gaussian distribution as sky background. On the other hand, wings of bright stars, faint stars and galaxies, cosmic rays, etc, distort the symmetric histogram of the pixel intensities, then the mean of the distribution is affected from this (i.e., it's no more equal to the sky background (mode)). However we can estimate the mode (sky background) from simple formula:

$$mode = 3 \times median - 2 \times mean \tag{2.10}$$

This formula is valid if the median is less than the mean. Else, it means that the distribution is small so the mean value can be estimated as mode.

2.4.4 Adding Up The Light

After determining the center of the star and background intensity, we can easily calculate the magnitude of the image.

$$m = zpt - 2.5logI \tag{2.11}$$

$$I = \sum I_{ij} - 0n_{pix}i_{sky} \tag{2.12}$$

Here zpt is a constant and its value is between 20-25, n_{pix} is the number of pixels in the aperture, i_{sky} is the background sky value, and the summation is carried out over those pixels.

2.4.5 Point Spread Function Photometry (PSF)

It's more appropriate to use this technique if the field of interest is crowded. There are two kinds of PSFs: (1) empiric, (2) model. We use only the data, in empiric PSF, on the other hand, in model PSF we use special functions such as Gaussian, Modified Lorentzian and Moffat. In the second kind of photometry in order to make a PSF, we pick several stars and relative to the magnitudes of these stars, we can calculate the magnitudes of the other stars.

2.4.6 Transformation To A Standard System

Comparing the relative magnitude of a star with the magnitude of a standard star, apparent magnitude of a star can be found. There is a formula that most

of the computer programs use

$$V_{std} = V_{instrument} + A_0 + A_1(B-V) + A_2X + A_3X(B-V) \tag{2.13}$$

The constants A_i are designated as below:

A_0 = the zeropoint - a measure of the sensitivity of the CCD/telescope system

A_1 = the color-term - a measure of how well the instrumental system approximates the standard system. In most circumstances A1 should be less than 0.1.

A_2 = the first order extinction coefficient - this depends on the atmospheric transmission and therefore varies from site to site and often from night to night.

A_3 = the second order extinction coefficient - this term is necessary, particularly for B, because extinction varies rapidly across the bandpass so that combined with the change in effective wavelength with spectral type, a variation in effective extinction with spectral type results.

X = air mass

B-V = color index of the standard star.

CHAPTER 3

TIME SERIES ANALYSIS AND POWER SPECTRAL METHODS

3.1 Discrete Fourier Transform

One of the main goal in astronomical data analysis is to detect a hidden signal in the presence of the noise with in a time series. Also finding the harmonic content can be considered as a second problem. In order to detect a hidden signal we use Fourier techniques. By applying Fourier transform one can decomposes a signal into sine waves. We can use continuous or discrete Fourier transform to detect the signal according to the data we use. However, astronomical data we obtain are in discrete units, so we should use discrete Fourier transform(DFT). If we say number of photons detected at a specific time interval k_m (m=0,...N-1) and take the number of data points as N then the Fourier transform f_n (n= -N/2,...N/2-1) of k_m becomes (van der Klis,1989);

$$\begin{aligned} f_n &= \frac{1}{N}\sum_{m=0}^{N-1} k_m e^{\frac{2\Pi i m n}{N}} \\ k_m &= \sum_{n=-N/2}^{N/2-1} f_n e^{\frac{-2\Pi i m n}{N}} \end{aligned} \tag{3.1}$$

Here k_m is related with time $t_m = \frac{mT}{N}$ with a time series length T and f_n

indicates a frequency $w_l \equiv 2\Pi\nu_n = \frac{2\Pi n}{T}$. We can find here that $t_m w_n = \frac{2\Pi mn}{N}$. So eqs above change;

$$\begin{aligned} f_n &= \frac{1}{N}\sum_m k_m e^{iw_n t_m} \\ k_m &= \sum_n f_n e^{-iw_n t_m} \end{aligned} \tag{3.2}$$

We can get a complete description of the discrete signal from DFT. The highest frequency needed for this complete description is

$$\nu_{N/2} = \frac{1}{2}N/T \tag{3.3}$$

which is called Nyquist frequency

Now we can define power spectrum as(van der Klis,1989);

$$P_n \equiv \frac{2}{N_{ph}}|f_n|^2 \tag{3.4}$$

where j=0,...,N/2 at zero freq $f_0 = \sum_m k_m \equiv N_{ph}$(total number of photons detected)

If we define the periodogram explicitly from above equation(Deeming, 1975);

$$P_k(w) = \frac{1}{N_0}\left[\left(\sum_m k_m \cos wt_j\right)^2 + \left(\sum_m k_m \sin wt_j\right)^2\right] \tag{3.5}$$

Consider our data k(t) have a sinusoidal frequency component and at w is equal to this frequency k(t) and sinusoidal terms come in phase and sums become large. However, at other component of frequencies the terms in the sum are randomly positive and negative and final sums become small.

There are two disadvantages of the DFT; statistical problems and spectral leakage. The cause of the statistical problem is that the noise can not be averaged out i.e., even more data added, the noise does not decrease in amplitude. However, when we add more data, the signal to noise ratio increases although, we cannot eliminate the noise. Expected powers due to the signal at signal frequency and due to the observational error are respectively;

$$\begin{aligned} < P_k > &= N_0(k_0/2)^2 \\ < P_R > &= < R >^2 = \sigma^2 \end{aligned} \tag{3.6}$$

so the signal to noise ratio becomes;

$$P = N_0(k_0/2\sigma_0)^2 \tag{3.7}$$

If a sinusoidal signal at w_0 appears at other frequencies as well as at w_0, we call this phenomenon as spectral leakage which arises from the finite amount of data. There is a special form of spectral leakage, called aliasing which is the leakage of power from high frequencies to lower frequencies. Aliasing appears much more in even sampled data. If the data we have is unevenly spaced aliasing would not be a serious problem.

A power spectrum consists of both noise and signal power and its hard to make a distinction between them. In order to construct a relationship between the noise and the signal power we can make a small assumption that signal power is a small perturbation from the level of noise, which leads us to consider noise

and signal power are independent quantities (van der Klis, 1989). Then total spectrum can be written as below:

$$P_j = P_{j,noise} + P_{j,signal} \tag{3.8}$$

The normalization given in Eq.3.4 is applied to the power spectrum, that if the photon counting data were pure Poissonian noise, then $P_{j,noise}$ distribution becomes χ^2 distribution with 2 degrees of freedom so that the probability for a given $P_{j,noise}$ to a certain threshold $P_{threshold}$ is given by (van der Klis, 1989)

$$Prob(P_{j,noise} > P_{threshold}) = Q(MWP_{threshold}|2MW), \tag{3.9}$$

where, W is the frequency bins following one another, M is the equal data set segments, $P_{threshold}$ is the minimum level at which a signal is significant and j=1,..,N/2-1. The integral probability of the χ^2 distribution is (van der Klis, 1989);

$$Q(\chi^2|\upsilon) \equiv \left[2^{\upsilon/2}\Gamma\left(\frac{\upsilon}{2}\right)\right]^{-1} \int_{\chi^2}^{\infty} t^{\frac{\upsilon}{2}-1} e^{-\frac{t}{2}} dt, \tag{3.10}$$

where υ is the number of degree of freedom and Γ is gama function. In the presence above equation we can define the detection level as

$$\frac{\epsilon}{N_{trial}} = Q(MWP_{detect}|2MW) \tag{3.11}$$

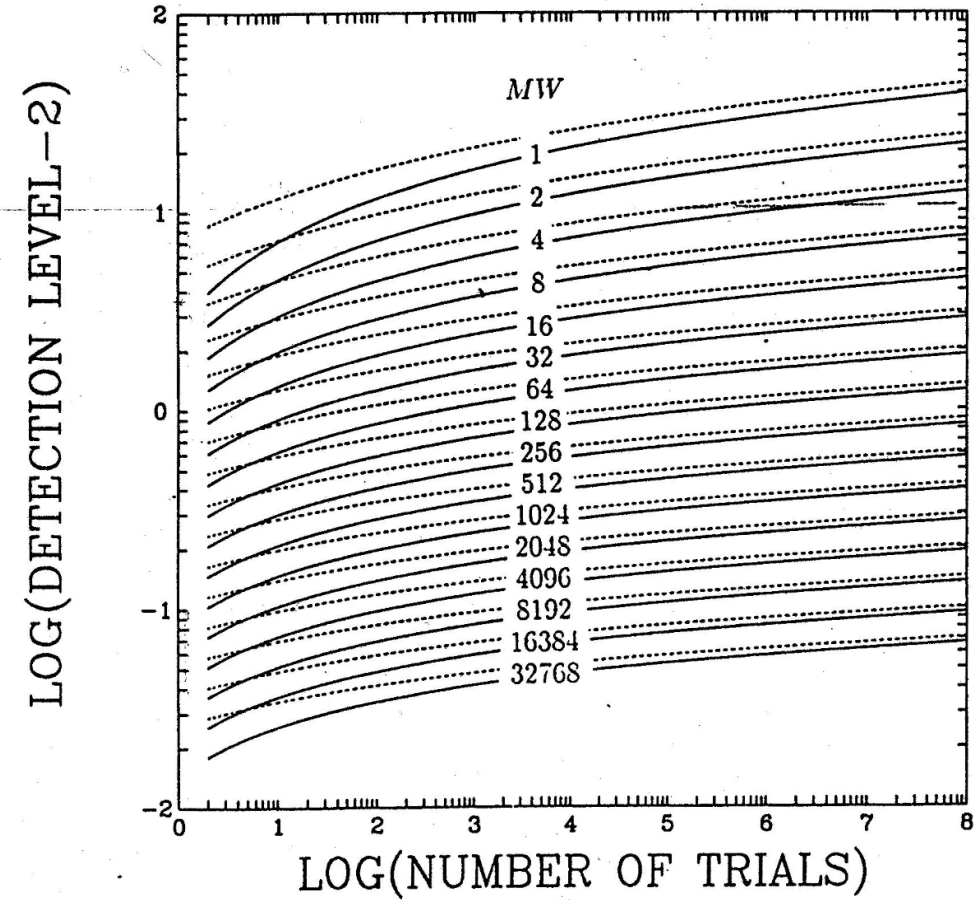

Figure 3.1: 99% (dashed lines) 90% (solid lines) confidence levels for different MW's.

3.2 Scargle Time Series Analysis

Scargle made an important contribution to time series analysis which includes a new definition in classical periodogram. It is a useful method to detect weak periodic signals in a noisy spectrum. Our observations are uncontrolled experiments and this method works very well in such experiments. Scargle method based on the least squares fitting of the sine function to the data (Scargle,1982). His approach is based on the introduction of the new shifted time points which provides orthogonality of the $sin(w\tau)$ and $cos(w\tau)$ functions.

$$\tau = t_j - \frac{1}{2w} \arctan \frac{\sum_j \sin 2wt_j}{\sum_j \cos 2wt_j} \tag{3.12}$$

Hence, Scargle spectrum becomes;

$$S_k(w) = \frac{1}{2} \left[\frac{\left(\sum_j k_j \cos w\tau\right)^2}{\sum_j \cos^2 w\tau} + \frac{\left(\sum_j k_j \sin w\tau\right)^2}{\sum_j \sin^2 w\tau} \right] \tag{3.13}$$

We want to find a power level z_0 that any power which exceeds this z_0 has significance as a detected signal. Scargle (1982), gives this detection threshold as following,

$$z_0 = -\ln \left[1 - (1 - p_0)^{1/N}\right] \tag{3.14}$$

CHAPTER 4

PHOTOMETRIC ANALYSIS OF V2275 CYG AND RW UMI

4.1 Photometric Analysis of V2275 Cyg

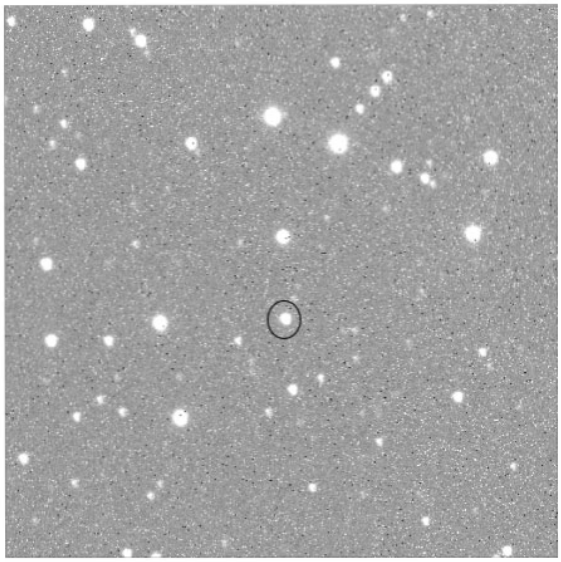

Figure 4.1: The field of the classical nova (V2275 Cyg). The nova is circled. The image was obtained on 2002.12.22. North is up, east is left.

V2275 Cyg(Nova Cyg 2001 was discovered at magnitude 8.8 on 2001 August(IAUC 7686), (IAUC 7687). The nova was found as a typical FE II-type nova because of the presence of FE II multiplets. At later stages, high energy coronal lines were found to dominate the spectrum with [Si X], [Si IX] and [Al

IX]. Finally, the nova defined to be belonging to "HE/N" subclass of novae defined by Williams(1992), because its optical spectrum dominated by broad lines of H,He and Ne (Kiss, L.L et al. 2002). The nova lies between 3 kpc and 8 kpc from the sun (Kiss, L.L et al. 2002).

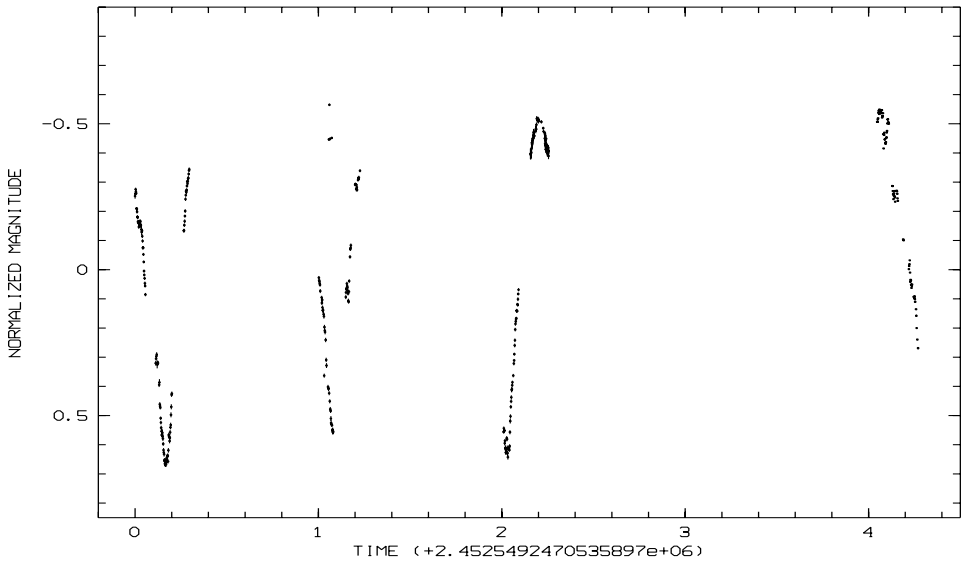

Figure 4.2: The light curve of V2275 Cyg obtained using the 1.5m telescope at TUG with R filter during the 4 nights in 2002 October. Errors are also included.

The raw data were obtained during 8 nights at Tubitak National Observatory(TUG), and reduced using standard procedures. Dark current frames and dome flat fields were obtained and averaged for each run. After the raw data was cleaned and calibrated for dark current and gain variations, the instrumental magnitudes of the nova and the four nearby comparison stars were derived by PSF fitting algorithm of DAOPHOT (Stetson,1987) and ALLSTAR within the MIDAS software package. The relative magnitudes were calculated using the four comparison stars and averaged to reduced scintillation effects. The observation

Table 4.1: The observations time table for V2275 Cyg

UT Date	Time of Start (HJD-245200)	Run Time (h)	Filter
020610	436.485	1.79	R
020612	438.486	1.81	R
021001	549.247	7.09	R
021002	550.252	5.30	R
021003	551.256	5.90	R
021005	553.294	5.34	R
021201	610.238	1.42	R
021222	631.189	2.90	R

dates and run durations for each night are given Table.4.1.

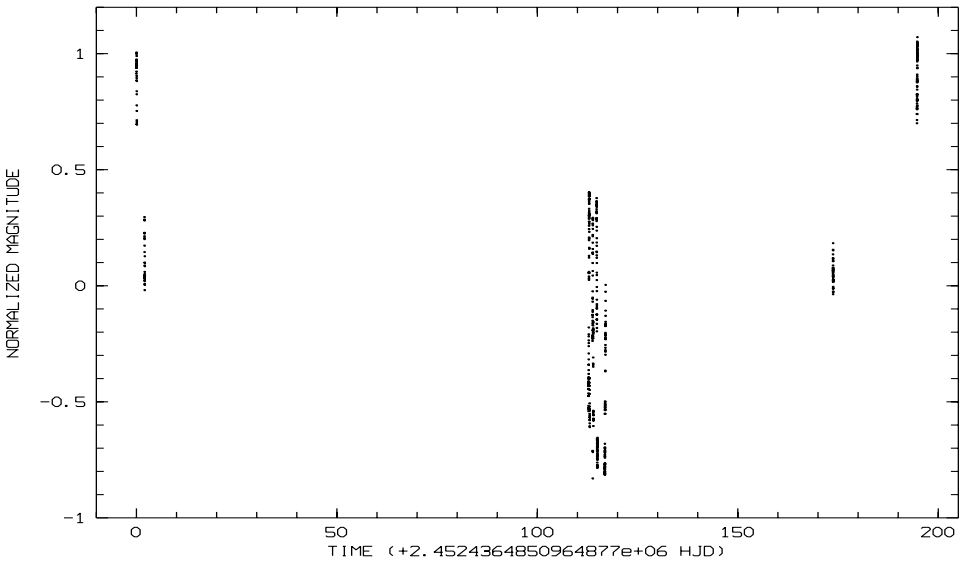

Figure 4.3: The light curve of V2275 Cyg obtained using the 1.5m telescope at TUG with R filter during the 8 nights in 2002. Errors are also included.

Fig.4.2 shows the light curve of four nights of observation obtained on 01-05 October 2002, where we can see the large magnitude variations and the detected maxima and minima. Fig.4.3 shows the complete light curve obtained for V2275 Cyg over the 8 nights at TUG.

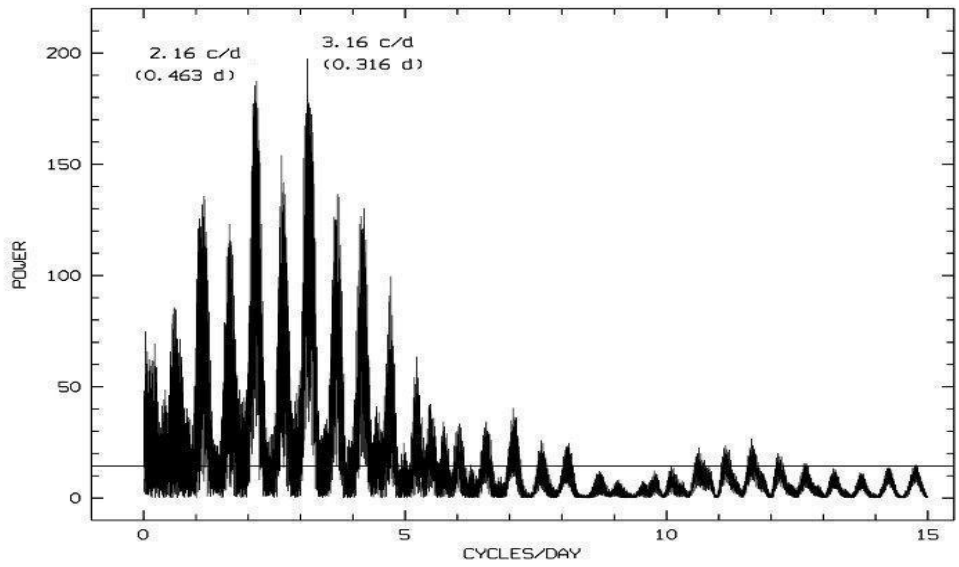

Figure 4.4: Power spectrum of V2275 Cyg obtained performing a transform of the entire time series data using the Scargle algorithm.

In order to recover the periodic variations in the light curve, we performed time series analysis using programs within the MIDAS software, which includes Discrete Fourier transform and Scargle time series analysis programs. We also normalized the light curves for each night by subtracting the mean in order to remove unwanted trends. In addition, we created synthetic light curves, by setting a constant value as magnitude and used the power spectrum of this data, to detect prominent artificial signals. These signals are subtracted from the original power spectrum by fitting an appropriate sine function. Removing these signals reduced the noise in the low frequency range, making real signals more apparent in the power spectrum. As a result, in Fig.4.4 we detect large variations in the light curve of this classical nova with a period of 0.316 ± 0.007 day. Which is also reported by our group (Balman et al 2003).

Actually, there are other peaks we can detect in the power spectrum of V2275 Cyg however, we cannot be sure that they are real signals. In order to make any meaningful comment on these peaks, more data and analyse are required.

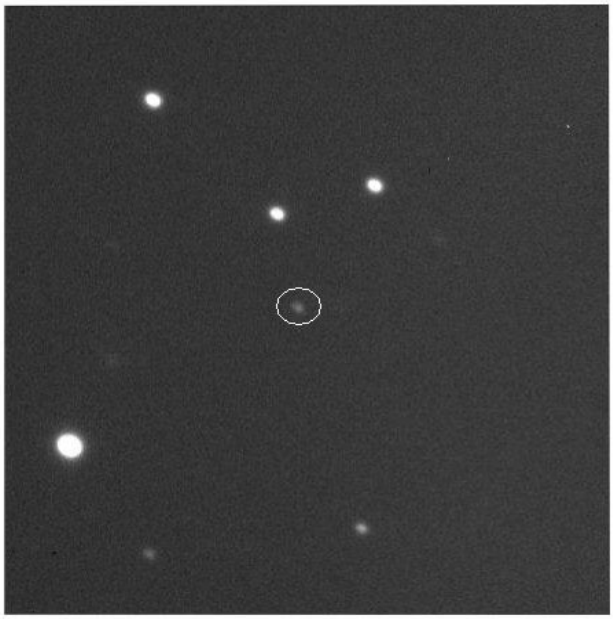

Figure 4.5: The field of the classical nova (RW UMi). The nova is circled. The image was obtained on 2001.09.16. North is up and east is left.

4.2 Photometric Analysis of Classical Nova RW UMi

RW UMi which had an outburst in 1956, is high galactic latitude classical nova (Retter and Lipkin, 2001). The apparent magnitude at maximum was $m_v = 6.0$ and decreased to $m_v = 11.5$ one year later (Kukarkin 1962). It's visual magnitude as an accreting CV is about $m_v = 21.0$ (Szcody et al. 1989). The spectra of RW UMi shows a blue continuum and H, HeI, HeII line emissions (Kaluzny and Chlebowsky 1989; Szkody et al. 1989; and Ringwald et al 1996). RW UMi is 5 ± 2 kpc away from our sun (Slavin et al 1995). We can see the complete 19 nights light curve of RW UMi in Fig.4.6. We have 11 nights of observations obtained with TUG and 8 nights of observation from 1 m telescope at WISE observatory see (Table 4.2). There are several detected periods of RW UMi: 117 ± 5 min

Table 4.2: The observations time table for RW UMi

UT Date	Time of Start (HJD-245200)	Run Time (h)	Filter	Observatory
010621	82.405	3.04	R	TUG
010623	84.390	2.73	R	TUG
010723	114.277	5.32	R	TUG
010724	115.280	5.25	R	TUG
010725	116.333	2.77	R	TUG
010815	137.312	2.80	R	TUG
010827	149.248	2.19	clear	WISE
010903	156.428	1.48	clear	WISE
010904	157.417	1.93	clear	WISE
010905	158.406	2.66	clear	WISE
010907	160.382	2.90	clear	WISE
010908	161.381	4.35	clear	WISE
010909	162.283	1.66	clear	WISE
010913	166.259	3.22	clear	WISE
010916	169.261	1.72	R	TUG
040527	1153.356	3.31	V	TUG
040528	1154.344	3.73	V	TUG
040529	1155.409	2.89	V	TUG
040530	1156.352	3.48	V	TUG

(Szkody et al. 1989), 113 ± 10 min (Howell et al. 1989) and 0.05912 ± 0.00015 d (1.4 hrs- Retter and Lipkin,2001) the orbital period. The last period found by Retter an Lipkin, below the CV's $2hr < P_{orb} < 3hr$ period gap and because there are only 3 detected CVs; V1974 Cyg 1992, GQ Mus 1983 and CP Pup 1942 (Ritter & Kolb 1998; Diaz & Bruch 1997), its important to work in detail with this object in order to understand the novae periodicities.

The photometric analysis of RW UMi is a rather difficult process because it has intrinsic irregularities in its light curve and small amplitude variations. When we investigate the power spectrum of RW UMi for different combinations of nights

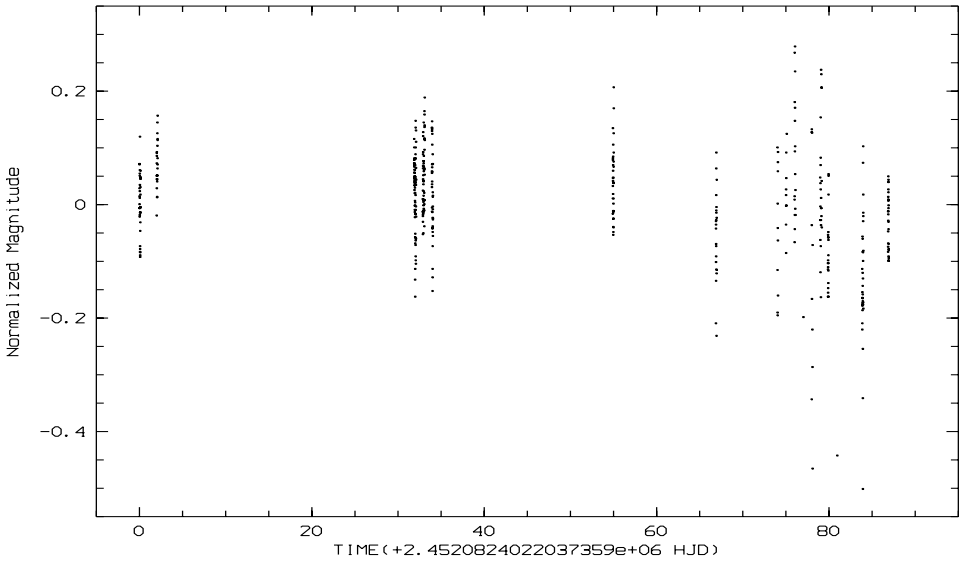

Figure 4.6: The light curve of RW UMi obtained using the 1.5m telescope at TUG and 1m telescope at WISE observatory with R filter during the 14 nights. Errors are also included.

we have interesting results. The last results we have reached provides us to make some discussion. If we classify the frequencies we detect from the whole data the orbital frequency becomes $\Omega = 12.23$, spin frequency becomes $\omega = 18, 48$ with periods $P_{orb} = 1.96 \pm 0.073h = 117.6 \pm 4.3$ min and $P_{spin} = 1.29 \pm 0.036h = 77.4 \pm 2.2$ min respectively. The other two frequencies can be considered as beat frequencies(orbital sidebands), $\omega - \Omega = 6.25 \sim 6.71$ and $2\omega - \Omega = 24.73$. All the significant frequencies detected from different power spectra which are obtained by using different filters and combination of these time series can be seen in Table.4.3 and in Figures.4.7, 4.8, 4.9, 4.10 and 4.11.

Observations of IPs shows us the existence of beat frequencies $\omega - \Omega$, $2\Omega - \omega$, $\omega + \Omega$ in their power spectrum (Warner 1995). These frequencies arise from several

Table 4.3: Detected significant frequencies and corresponding periods for RW UMi

Filter	Significant Frequencies (Cycles/Day)	Corresponding Periods (hr)
	6.80	3.53
R	13.23	1.81
	17.86	1.34
clear	6.28	3.82
	13.60	1.76
V	14.20	1.69
	24.61	0.97
R and clear	6.83	3.51
	11.15	2.15
	19.48	1.23
R, clear and V	6.80	3.53
	12.23	1.96
	18.48	1.29
	24.73	0.97

possible reasons: 1) overflow of considerable amount of accreting material over the accretion disc, which goes straight on to poles of the WD following magnetic field lines as a stream that alternates from one pole to the other at the beat period (Hellier 1991). 2) interaction of magnetic field of WD with accretion disc which is distorted by tidal forces of the secondary. Saying in other words, tidally induced spiral shocks can interact with the matter at the magnetosphere of the WD resulting with beat periods between the WD spin and binary orbital periods (Murray et al. 1999a). The beat frequency and sidebands predicted from our data show quite similarities to the type of IPs which yields evidence that RW UMi can be an intermediate polar.

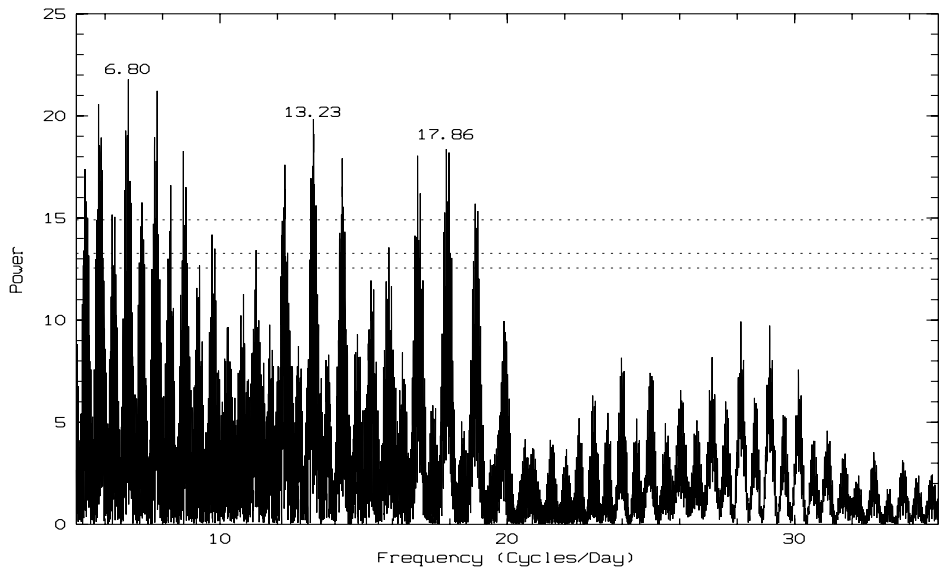

Figure 4.7: Power spectrum of RW UMi obtained performing a transform of the time series data obtained by R filter using the Scargle algorithm.

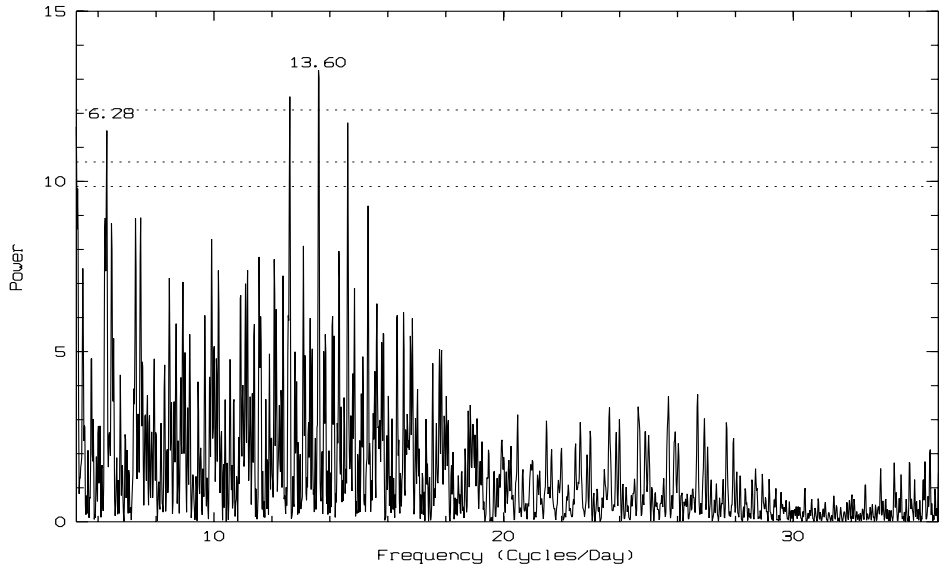

Figure 4.8: Power spectrum of RW UMi obtained performing a transform of the time series data obtained by clear filter using the Scargle algorithm.

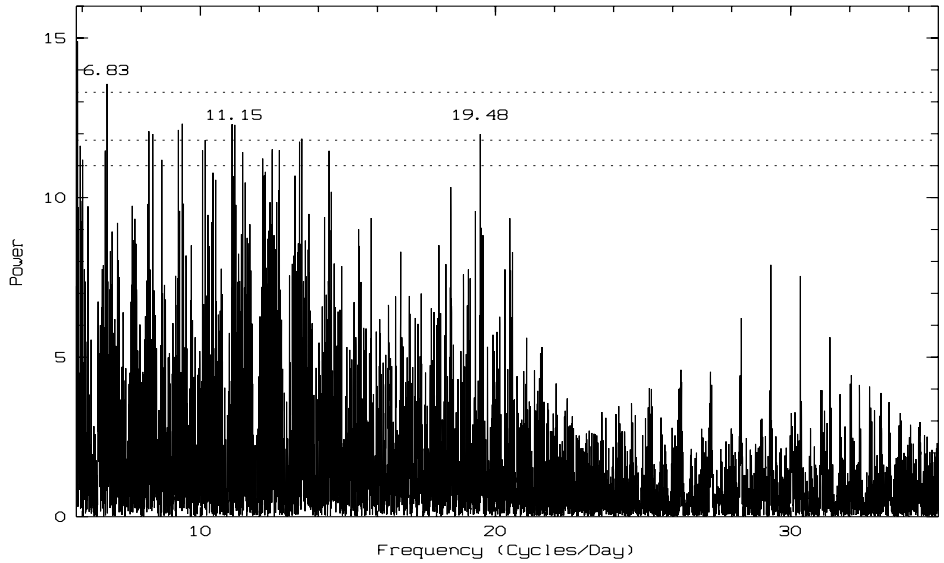

Figure 4.9: Power spectrum of RW UMi obtained performing a transform of the time series data obtained by combination of R and clear filter using the Scargle algorithm.

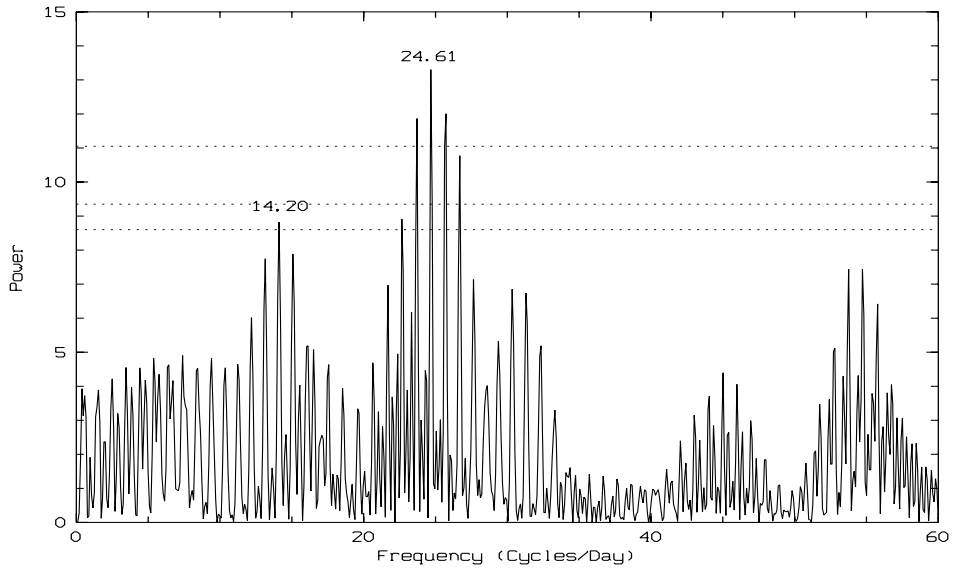

Figure 4.10: Power spectrum of RW UMi obtained performing a transform of the time series data obtained by V filter using the Scargle algorithm.

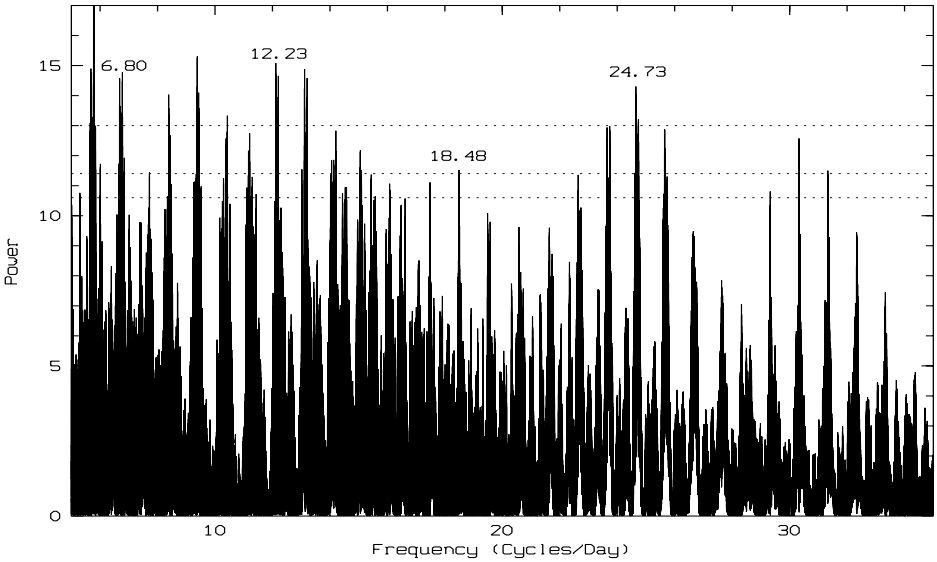

Figure 4.11: Power spectrum of RW UMi obtained performing a transform of the entire time series data using the Scargle algorithm.

CHAPTER 5

CONCLUSION

In this thesis, we performed time series analysis of two classical novae V2275 Cyg and RW UMi. Beforehand, we made a review of basic photometry techniques and data reduction methods. In addition, we briefly described discrete fourier transform and Scargle time series analysis which is a special kind of DFT.

The power spectrum of V2275 Cyg shows us that a period 0.316 ± 0.007 day which is most probably the orbital period of the system because it is the strongest period in the power spectrum. We have been discovered deep modulations in the light curve of this classical novae. The observed variations in V2275 Cyg can be explained by light coming from the secondary star in the system illuminated by white dwarf. The shape of the modulation is sinusoidal which nearly fits the light curve of V2275 Cyg.

Time series analysis of RW UMi gives us the following results:

1) We find possible period candidates in our power spectrum which we assume $P_{orb} = 1.96 \pm 0.073h = 117.6 \pm 4.3$ min as the orbital period and $P_{spin} = 1.29 \pm 0.036h = 77.4 \pm 2.2$ min as the spin period. The orbital period we claim is also consistent with previously detected periodicities such as; 117 ± 5 min (Szkody et

al. 1989), 113 ± 10 min (Howell et al. 1989). However we are not able to detect the 1.4 h orbital period (Retter and Lipkin 2001) in our analysis.

2) We also find a dominant peak in the power spectrum of RW UMi that $2\omega - \Omega = 24.73$ which we conclude that it can be a beat frequency with a period $P_{beat} = 1.011$ h. This kind of beat frequencies are generally seen in intermediate polar type cataclysmic variables. For example, in AO Psc (van der Woerd, de Kool and van Paradijs 1984) the power spectrum shows modulation at frequencies $\omega_{spin} - 2\Omega_{orb}$ to $\omega_{spin} + 2\Omega_{orb}$. Additionally $\omega_{spin} - \Omega_{orb}$, $\omega_{spin} + \Omega_{orb}$ and $\omega_{spin} - 2\Omega_{orb}$ frequencies have been detected in AO Psc (Hellier, Cooper and Mason 1991), TX Col (Buckley and Tuohy 1989) and FO Aqr (de Martino et al. 1993). Theoretically $2\omega - \Omega$ frequencies are recovered in discless intermediate polar systems in which matter transferred from secondary to both of the poles of the WD by a stream (Murray et al. 1999a). Also we find another side band frequency $\omega_{spin} - \Omega_{orb} = 6.19$ c/d which is close to the frequency 6.77 c/d that we detect in our power spectrum. Presence of this beat frequency indicates a discless IP system with a mass transfer stream to only one of the poles of WD. A similar prediction was made by Bianchini 2001. He also finds a beat frequency about $\omega_{spin} - \Omega_{orb} = 26.50$ which is close to our beat frequency.

Our results have large errors on the periods due to low modulation depths and aliasing in the power spectra but encourage us to make further observations in order to make confirmation.

REFERENCES

[1] Balman S., Yilmaz M.A., Retter A., Ak T., Saygac T., Esenoglu H., Aslan Z., IAUC, 8074

[2] Buckley D.A.H., Tuohy, I.R., 1989, ApJ., 344,376

[3] Diaz M.P., Bruch A., 1997, A&A., 332, 807

[4] de Martino D., Buckley D.A.H., Mouchet M., Mukai K. 1994, A&A., 284, 125

[5] Harvey D., Skillman D.R., Patterson J., Ringwald F.A., 1995, PASP, 107, 551

[6] Hellier C., 1991, MNRAS, 251, 693

[7] Howell S., Dobrzycka D., Szkody P., and Keidl T., 1991 PASP, 107, 324

[8] Howell S., 1992, ASP Conference Series, Vol.23

[9] Kaluzny J., Chlebowski T.,1989, Acta Astron, 39,35

[10] Kiss L.L., Gogh N., Vinko J., Furezs G., Csak B., DeBond H., Thomson J.R., Derekas A., 2002, A&A, 384, 982

[11] Klis M., 1989, in Timing Neutron Stars, eds. H. ogelman and E.P.J. van den Heuvel, Kluver Academic Publishers

[12] Kukarkin B.B.,1962, IBVS, 18

[13] Murray J.R., Armitage P.J., Ferrario L., 1999, MNRAS, 302,189

[14] Nakamura A., 2001 IAUC, 7686

[15] Payne-Gaposchkin C., 1957, The Galactic Novae (New York : Dover)

[16] Retter A., Lipkin Y., 2001, A&A., 365, 508

[17] Ringwald F. A., Naylor T., Mukai K., 1996, MNRAS 281, 192

[18] Ritter H., Kolb U., 1998, A&A., 129,83

[19] Scargle J.D., 1982, ApJ, 263, 835

[20] Slavin A. J., O'brien T.T., Dunlop J.S., 1995, MNRAS, 276, 353

[21] Stetson P. B., 1987, PASP, 99, 191

[22] Szkody P., Howell S., Mateo M., Kreidl T.J., 1989, PASP, 101, 899

[23] Tago A., 2001, IAUC, 7686

[24] van der Woerd H., de Kool M., van Paradijs J., 1984, A A., 131, 137

[25] Ventruni C.C., Lynch D.K., Rudy R.J., Mazud S., 2002, IAUC, 7940

[26] Warner B., 1995, Cataclysmic Variable Stars, Cambridge University Press, Cambridge

[27] Whitehurst R., King A., 1991, MNRAS, 249, 25